Polymer Degradation and Stability 134 (2016) 245–250

Contents lists available at ScienceDirect

Polymer Degradation and Stability

journal homepage: www.elsevier.com/locate/polydegstab

Short communication

The effect of hole transport layer on the thermal stability of inverted polymer solar cells

Ming-Chih Lin [a], Yu-Ching Huang [a, b, *], Chia-Te Yen [b], Cheng-Si Tsao [b, c], Yee-Wen Yen [a]

[a] Department of Materials Science and Engineering, National Taiwan University of Science and Technology, Taipei, 10607, Taiwan, ROC
[b] Institute of Nuclear Energy Research, Longtan, Taoyuan, 32546, Taiwan, ROC
[c] Department of Materials Science and Engineering, National Taiwan University, Taipei, 10607, Taiwan, ROC

ARTICLE INFO

Article history:
Received 2 May 2016
Received in revised form
13 October 2016
Accepted 21 October 2016
Available online 22 October 2016

Keywords:
Polymer solar cells
Hole transport layer
P3HT
PEDOT:PSS
Thermal stability

ABSTRACT

In this article, the effect of hole transport layer (HTL) on the thermal stability of inverted polymer solar cells (PSCs) consisting of the blend of poly(3-hexylthiophene) (P3HT) and (6,6)-phenyl-C_{60} butyric acid methyl ester fullerene derivative (PCBM) as active layer (AL) is investigated. The two conventional HTLs, poly(3,4-ethylenedioxythiophene):polystyrene sulfonate (PEDOT:PSS) and MoO_3, were used in this study to demonstrate the effect of HTLs on the thermal stability of PSCs. The inverted devices were heated at 80 −110 °C as accelerated test for different time intervals to illustrate the temporal variation of performance. The different temporal behaviors during (1) metastable period and (2) thermally unstable period are described here. Moreover, the effect of photoactive film thickness on the thermal stability of devices based on the two HTLs was considered. This study shows that the spin- and spray-coated devices exhibit different characteristics of thermal stability for the PSCs with MoO_3 and PEDOT:PSS as HTLs, respectively. The temporal behavior caused by the effect of HTL during the thermally-unstable period is quantitatively studied. This study could provide vital information required to develop high durability in commercial PSCs.

1. Introduction

Polymer solar cells (PSCs) have attracted a lot of attention in the past decades due to several advantages they offer, such as light weight, low energy requirement in manufacturing, low manufacturing costs, solution processability, ease of large-area fabrication, and mechanical flexibility [1–3]. Many research groups have made efforts to improve the power conversion efficiency (PCE) of PSCs, and most of the groups focus on the synthesis of low band-gap polymers to effectively harvest incident photons [4–7], improving the bulk heterojunction structure (BHJ) of PSCs [8–10], and enhancing charge transport by interfacial engineering [11–13]. In the conventional PSC devices, the conducting polymer, poly(3,4-ethylenedioxythiophene):polystyrene sulfonate (PEDOT:PSS), is usually deposited between the AL and ITO electrode as the hole transporting layer (HTL), and the low work function (WF) metal is used as the metal electrode. However, the stability of these conventional PSCs is limited due to the low WF metal electrode and ITO degradation by the acidic nature of PEDOT:PSS [14]. In addition, the hygroscopic nature of PEDOT:PSS would adsorb water molecules, which diffuse through the active layer and to the electrode and cause the oxidation of the low work function electrode [15]. Therefore, the inverted PSCs with good device stability are broadly investigated, aimed at PSC commercialization. Inverted PSCs, in general, use metal oxide, such as ZnO, TiO_x, as the electron transport layer (ETL) between ITO and AL. In addition, less air sensitive high WF metal electrodes, such as Au or Ag, are used in the inverted PSC. However, most of the inverted PSCs show poor stability after prolonged exposure to heat due to the aggregation of PCBM [16]. Considering the fact that the AL of PSCs is subjected to serious phase separation due to high temperature, enhancing the thermal stability is of critical importance. In order to improve the thermal stability of PSCs by controlling the AL morphology, many strategies have been devised, which include addition of polymer compatibilizers [17], and the use of fullerene derivative [18–20] or thermally cross-linkable donor or acceptor materials within the AL [21,22]. By applying these strategies, the thermal stability of PSCs could be improved dramatically even at an elevated temperature of

* Corresponding author. Institute of Nuclear Energy Research, Longtan, Taoyuan, 32546, Taiwan, ROC.
E-mail address: huangyc@iner.gov.tw (Y.-C. Huang).

http://dx.doi.org/10.1016/j.polymdegradstab.2016.10.014
0141-3910/

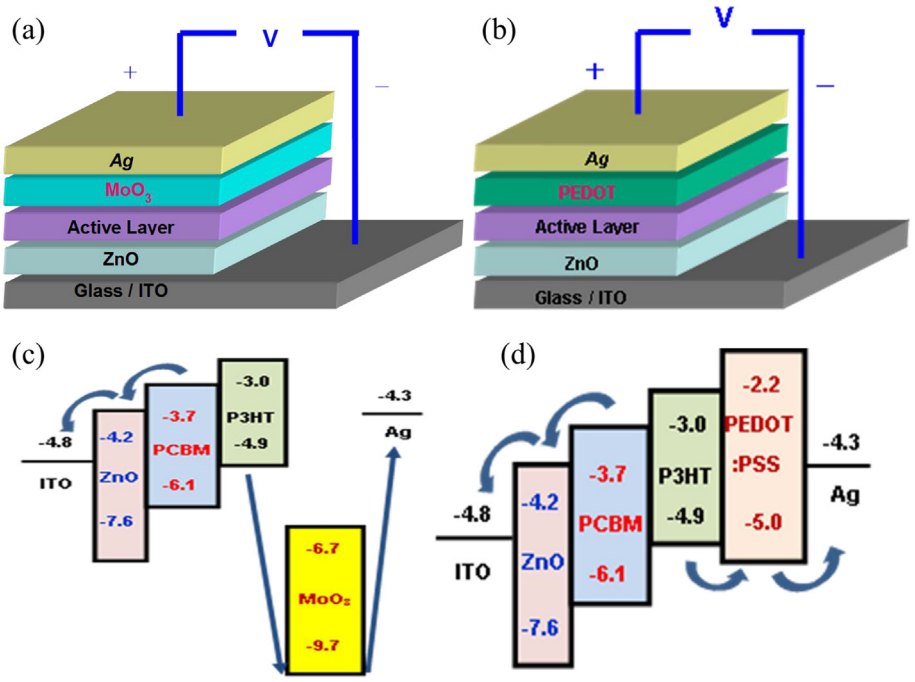

Fig. 1. The schematics of devices and the corresponding bandgap diagram based on (a, c) MoO_3 and (b, d) PEDOT:PSS as the HTL.

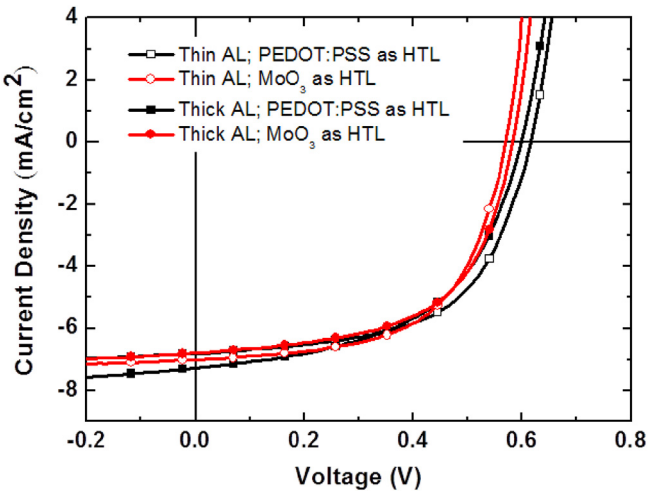

Fig. 2. Current-voltage curves of four types of spin-coated devices based on two active layer thicknesses and two HTLs (PEDOT:PSS and MoO_3).

over 150 °C. However, most of these studies focus on the control of AL morphology evolution. There are only few studies describing the thermal stability due to the interfacial interaction between AL and HTL. As reported in these studies such interface can effectively influence the performance of PSCs. It might be expected that the interfacial interaction between different HTLs and AL can cause the degradation of performance due to thermal effect that served as the motivation behind the present study. On the other hand, the P3HT:PCBM blend is generally adopted as the model system with good stability. Herein, the effect of HTLs on the thermal stability of PSCs based on inverted structures with different thicknesses of AL is reported. The two commonly used HTLs, PEDOT:PSS and MoO_3, were adopted in this study to demonstrate the different thermal stability behavior. The PEDOT:PSS and MoO_3 devices were prepared using spin- and spray-coated processes, respectively. The results of this research open up new venues for high thermal stability PSCs.

2. Experiment

2.1. Materials

P3HT and PCBM were purchased from Rieke Metals. Indium tin oxide (ITO) coated glass substrate was used as transparent electrode and was obtained from Optical Filter Ltd (EMI-ito 15). The ZnO ETL was synthesized by sol-gel method, and the ZnO precursor was prepared as reported in our previous study [23]. The two HTL materials, PEDOT:PSS and MoO_3, were purchased from Heraeus (Clevios AI 4083) and Aldrich, respectively.

Table 1
Performance characteristics of spin- and spray-coated devices based on two HTLs (PEDOT:PSS and MoO_3).

AL concentration (mg/ml)	HTL	J_{sc} (mA/cm^2)	V_{oc} (V)	FF (%)	PCE (%)	PCE_{max} (%)
Spin devices						
10	PEDOT:PSS	6.63 ± 0.15	0.62 ± 0.00	57.3 ± 0.7	2.33 ± 0.04	2.4
	MoO_3	7.03 ± 0.09	0.57 ± 0.00	58.3 ± 0.9	2.33 ± 0.04	2.4
15	PEDOT:PSS	7.21 ± 0.08	0.61 ± 0.01	52.9 ± 0.1	2.30 ± 0.01	2.3
	MoO_3	6.75 ± 0.12	0.58 ± 0.00	56.0 ± 1.6	2.20 ± 0.07	2.3
Spray devices						
10	PEDOT:PSS	8.76 ± 0.09	0.58 ± 0.00	52.6 ± 1.3	2.68 ± 0.10	2.80
	MoO_3	8.64 ± 0.07	0.59 ± 0.00	54.5 ± 2.3	2.78 ± 0.13	2.90

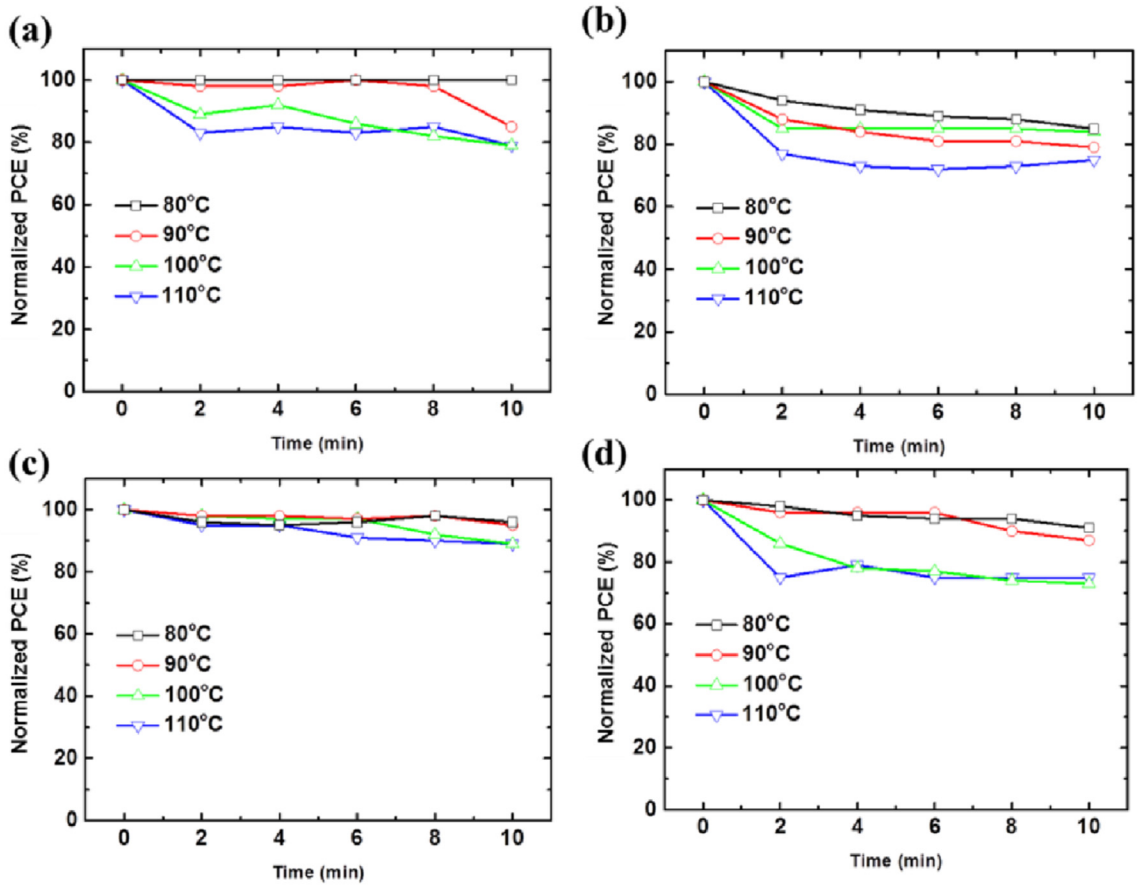

Fig. 3. Temporal variations of four types of spin-coated devices during thermal stability test: (a) Thin AL/PEDOT:PSS, (b) Thin AL/MoO_3, (c) Thick AL/PEDOT:PSS, (d) Thick AL/MoO_3.

2.2. Device fabrication

Inverted structure PSCs were used in this study. ITO-coated glass was cleaned by acetone and isopropanol sequentially in an ultrasonic cleaner. Then, ZnO ETL was fabricated by coating ZnO precursor onto a cleaned ITO glass, and calcining at 150 °C for 1 h. The photoactive layer consisting of P3HT and PCBM in 1:1 wt/wt ratio was dissolved in o-xylene and stirred at 50 °C overnight. The AL was deposited on the ZnO layer and annealed at 130 °C for 10 min in air. The thermal annealing of all ALs is referred to as the pre-annealing process herein. The two hole transporting layers, PEDOT:PSS and MoO_3, used in this study were deposited via spin coating and thermal evaporating, respectively. The corresponding film thicknesses of PEDOT:PSS and MoO_3 were ~40 nm and 3 nm. Finally, the silver electrode was thermally evaporated on the HTL. The device configuration of the two main types of inverted structures with MoO_3 and PEDOT:PSS as HTLs, respectively, is shown in Fig. 1(a) and (b). The corresponding energy level diagram is presented in Fig. 1(c) and (d) [24,25]. For each type HTL of devices, two types, a thin and thick AL, were prepared using polymer concentrations of 10 and 15 mg mL^{-1}, respectively, to include the thickness effect. The corresponding AL film thicknesses for 10 and 15 mg mL^{-1} are ~100 (thin AL) and 150 (thick AL) nm. Moreover, the ETL, AL, and HTL of these four types of PSC devices were prepared using the full spin- and spray-coated techniques, respectively as described in our previous literature [26,27]. The AL film thickness of spray-coated devices is ~250 nm.

2.3. Device characterization and thermal stability test

The PCE of all prepared devices was measured under AM 1.5G illumination at 100 mW/cm^2 using a solar simulation (Abet Sun 2000). The device thermal stability tests for the spin- and spray-coated devices without encapsulation were performed under ambient atmosphere. These devices with different HTLs and

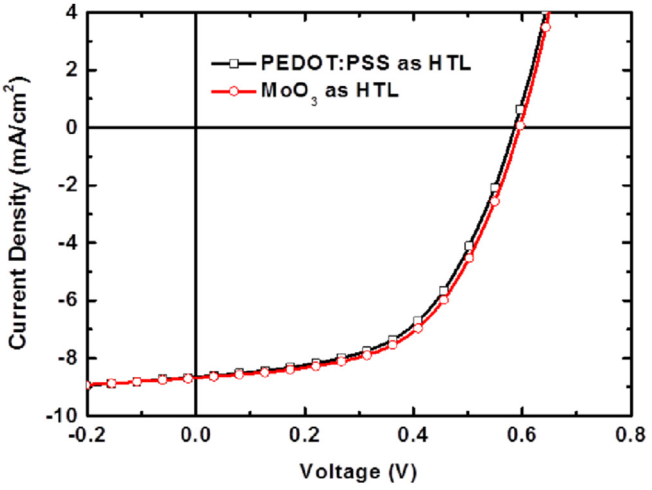

Fig. 4. Current-voltage curves of spray-coated devices based on two HTLs of PEDOT:PSS and MoO_3.

thicknesses were thermally treated at various temperatures (80, 90, 100, and 110 °C), respectively, for different periods of time, as the accelerated test to observe the PCE changes. It is worthy to note that the thermal treatment was performed on the devices (i.e., HTL and silver electrode were concurrently heated). Thus, the effect of HTL on the thermal stability is demonstrated in this study.

3. Results and discussion

The current density-voltage (J-V) curves and performance characteristics of these four types of spin-coated devices are shown in Fig. 2 and Table 1, respectively. Each datum of Table 1 was averaged based on 12 samples. The short circuit current (J_{sc}) and the fill factor (FF) were almost the same. The open-circuit voltage (V_{oc}) values of the devices with PEDOT:PSS HTL was slightly higher than those of the devices with MoO_3 HTL. The device with thin and thick AL showed a compatible PCE of ~2.3%.

The thermal stability of PSC caused by the different HTLs and AL thickness would be an interesting subject for future practical applications. At first, the thermal stability of the spin-coated devices was tested without encapsulation in an oven under an ambient condition for the initial evaluation to screen the parameters influenced by the thickness effect. The thermal stability test of the spin-coated devices as accelerated test was carried out at 80, 90, 100, and 110 °C for 2, 4, 6, 8, and 10 min, respectively. The consideration adopted with the un-encapsulation is to shorten the test time by including the degradation of humidity (~20% relative humidity in the high-temperature oven environment). The temporal evolution of PCEs during the thermal stability test is shown in Fig. 3. It is observed that all the degradation curves due to the thermal effect exhibit an initial decay (during the first 2 min) and then stabilizes during this period at different temperatures. This is called the "metastable period". It is different from the typical thermally-unstable stage. From Fig. 3(b) and (d), it is observed that the degradation of the MoO_3-based devices with thin and thick active layer dropped dramatically down to ~80% of the initial value (for the most serve case) during the first 2 min of storage at 110 °C. However, when compared with that of the PEDOT:PSS-based devices with thick active layer, as shown in Fig. 3(d), the initial loss and the subsequent saturation behavior of degradation of the devices still remained above 90% with respect to the initial value at 110 °C. The remarkable decay behavior of MoO_3—based devices can be explained by the phenomenon of thermal diffusion of metal atoms into the AL from the MoO_3 layer [28]. In contrast, the PEDOT:PSS-based devices with thick AL are able to retain relatively better thermal stability and PCE. It can thus be concluded that thick AL can have enough depth space to form a favorable interface with PEDOT:PSS layer, the neighboring zone, and effective BHJ structure. Therefore, the thick AL produced by the spray-coated process was adopted for the subsequent step to exclude the thickness effect.

The aim target of this study was to improve thermal stability of the spray-coated devices because of their commercial potential for large-area and mass-production fabrication. The J-V curves and performance characteristics of the spray-coated devices are shown in Fig. 4 and listed in Table 1. The periods of heating at 80, 90, 100, and 110 °C lasted for up to ~500 min to investigate the degradation behavior during the thermally-unstable stage. According to the previous literature [29], the variation of degradation behavior significantly depends on the combination of materials used. We demonstrate the temporal evolution of PCEs during the thermally-unstable stage, as shown in Fig. 5 and 6. Fig. 5(a) shows the PCE degradation curves of the spray-coated PEDOT:PSS-based devices.

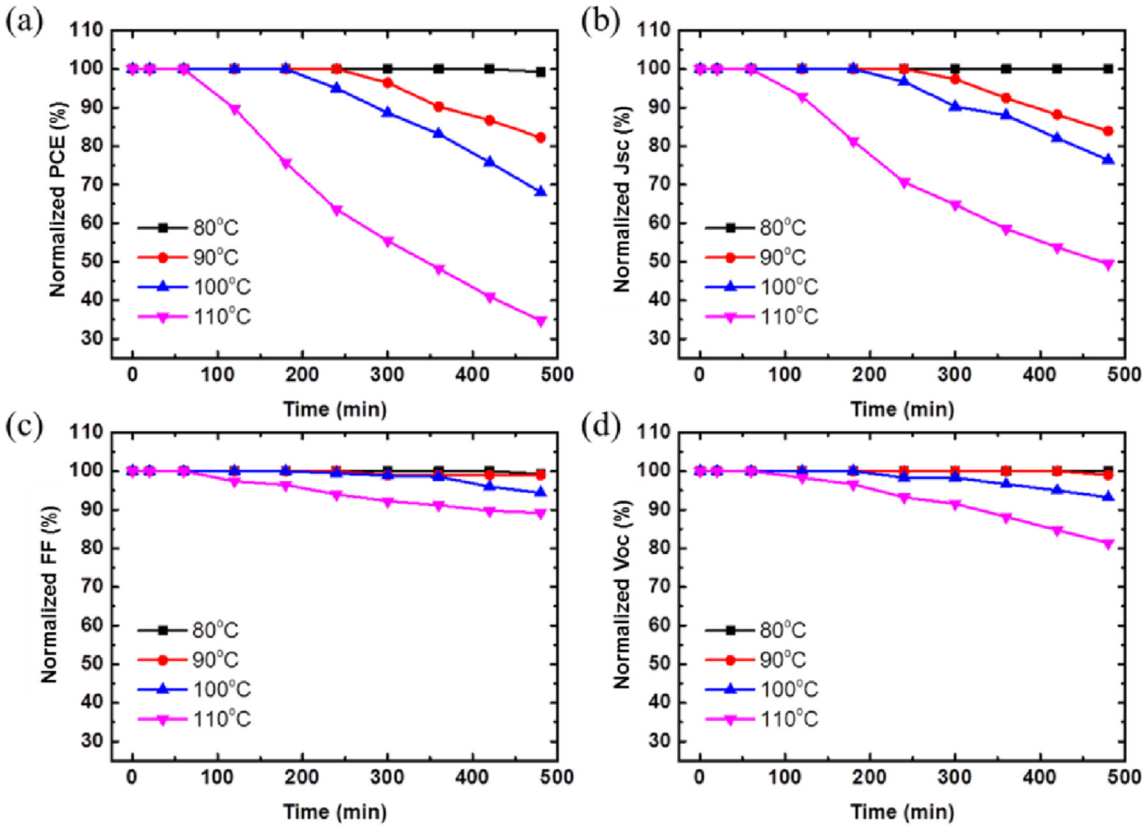

Fig. 5. Temporal evolutions in (a) PCE, (b) J_{sc}, (c) FF and (d) V_{oc} for the spray-coated devices based on PEDOT:PSS HTL during thermally unstable period at 80, 90, 100 and 110 °C.

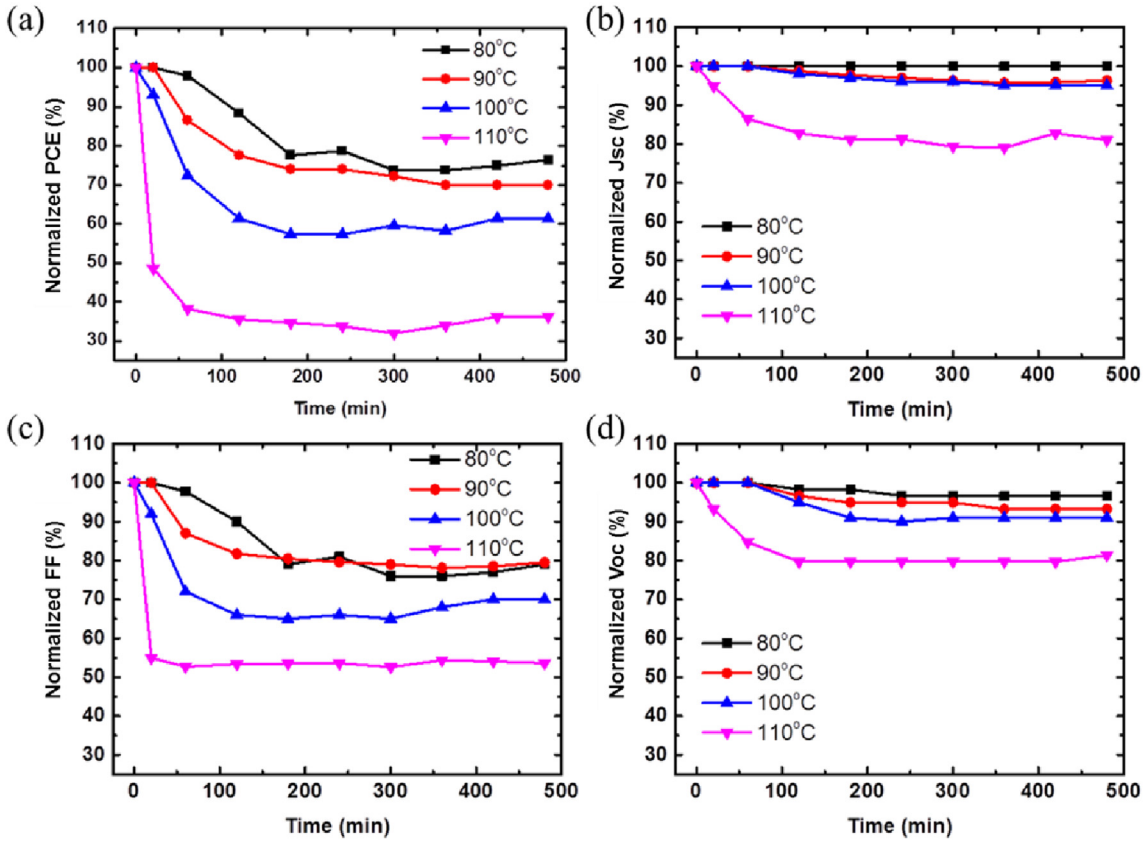

Fig. 6. Temporal evolutions in (a) PCE, (b) J_{sc}, (c) FF and (d) V_{oc} for the spray-coated devices based on MoO_3 HTL during thermally unstable period at 80, 90, 100 and 110 °C.

The evolutions of the corresponding J_{sc}, V_{oc} and FF are shown in Fig. 5(b)–(d), respectively. The PCE degradation trend of PEDOT:PSS-based devices can be divided into two states: (1) an initial plateau in the PCE and then (2) a monotonic decay. This is in accordance with the results of S. Sakkopoulos et al. [30], reporting that the conductivity of PEDOT:PSS at high heating temperature initially increases due to the improvement of the crystallinity, and then decreases with heating time [30]. They inferred that the reduced conductivity is resulted from the irreversible changes of the polymer backbone in the presence of oxygen and moisture. The change of PEDOT:PSS conductivity under heat is reflected by the J_{sc} behavior as shown in Fig. 5(b). The PCE degradation is mainly resulted from the J_{sc} variation. For the heating period of ~400 min, the PCE degradation increases with increasing temperature (reaches ~80%, ~65%, and ~40% of the initial PCE at 90 °C, 100 °C and 110 °C, respectively). It is a noteworthy feature that the PEDOT:PSS-based devices aged at 80 °C still present the same PCE as initial samples after ~500 min. This result is commented that 80 °C is a recommended temperature for performing thermal degradation of organic photovoltaics [31].

On the contrary, the decay trend of MoO_3-based devices is substantially different from that of PEDOT:PSS-based devices, as shown in Fig. 6. The PCE degradation trend of MoO_3-based devices shows the reduction of PCE mainly occurs at initial heating stage and then exhibits a slow-decay or saturation-like behavior. At the initial heating period, the PCE decay increases with the elevation of heating temperature. With an increase in the heating temperature from 90 °C to 110 °C, the PCE of MoO_3-based devices dramatically drop from 25% to 65%, and the degradation time of PCE is accelerated from 200 min to 10 min. The evolutions of the corresponding J_{sc}, FF and V_{oc} are shown in Fig. 6(b)–(d), respectively. It can be observed that the FF is the main reason for the PCE degradation. The pronounced FF decay could be attributed to the thermal diffusion of metal atoms into the photoactive layer. In addition, MoO_3-based devices display an apparent V_{oc} decay at the initial heating state (~200 min, Fig. 6(d)) as compared to that of PEDOT:PSS-based devices. The decline in V_{oc} is consistently similar to the results previously reported, which is attributed to the interfacial degradation [29]. It is worthy to note that among the devices treated at 110 °C for more than 450 min, the saturation curve of MoO_3-based devices crosses the degradation curve of PEDOT:PSS-based devices, showing a better thermal stability with time in the reverse order. However, for the devices treated at the low heating temperature (80 and 90 °C) for more than 450 min, the thermal stability of PEDOT:PSS-based devices is superior to that of MoO_3-based devices.

4. Conclusions

The spin- and spray-coated devices demonstrate similar behaviors of thermal stability. The different HTLs cause the distinctive characteristics of temporal evolution of PCE during (1) the metastable period and (2) the thermally-unstable period when the accelerated test at 80–110 °C for different lengths of time is performed. A thick AL could provide a favorable interface and BHJ structure considering the combination of HTL and thickness effects as a whole.

References

[1] Y.-W. Su, S.-C. Lan, K.-H. Wei, Organic photovoltaics, Mater. Today 15 (12) (2012) 554–562.
[2] L. Dou, J. You, Z. Hong, Z. Xu, G. Li, R.A. Street, Y. Yang, 25th Anniversary

article: a decade of organic/polymeric photovoltaic research, Adv. Mater. 25 (46) (2013) 6642–6671.
[3] L. Lu, T. Zheng, Q. Wu, A.M. Schneider, D. Zhao, L. Yu, Recent advances in bulk heterojunction polymer solar cells, Chem. Rev. 115 (23) (2015) 12666–12731.
[4] Y. Liang, Z. Xu, J. Xia, S.T. Tsai, Y. Wu, G. Li, C. Ray, L. Yu, For the bright future-bulk heterojunction polymer solar cells with power conversion efficiency of 7.4%, Adv. Mater. 22 (20) (2010) E135–E138.
[5] K.H. Ong, S.L. Lim, H.S. Tan, H.K. Wong, J. Li, Z. Ma, L.C. Moh, S.H. Lim, J.C. de Mello, Z.K. Chen, A versatile low bandgap polymer for air-stable, high-mobility field-effect transistors and efficient polymer solar cells, Adv. Mater. 23 (11) (2011) 1409–1413.
[6] T.-Y. Chu, S.-W. Tsang, J. Zhou, P.G. Verly, J. Lu, S. Beaupré, M. Leclerc, Y. Tao, High-efficiency inverted solar cells based on a low bandgap polymer with excellent air stability, Sol. Energy Mater. Sol. Cells 96 (2012) 155–159.
[7] X. Guo, M. Zhang, W. Ma, L. Ye, S. Zhang, S. Liu, H. Ade, F. Huang, J. Hou, Enhanced photovoltaic performance by modulating surface composition in bulk heterojunction polymer solar cells based on PBDTTT-C-T/$PC_{71}BM$, Adv. Mater. 26 (24) (2014) 4043–4049.
[8] Y.-C. Huang, C.-S. Tsao, C.-M. Chuang, C.-H. Lee, F.-H. Hsu, H.-C. Cha, C.-Y. Chen, T.-H. Lin, C.-J. Su, U.S. Jeng, W.-F. Su, Small- and wide-angle x-ray scattering characterization of bulk heterojunction polymer solar cells with different fullerene derivatives, J. Phys. Chem. C 116 (18) (2012) 10238–10244.
[9] H.-C. Liao, C.-S. Tsao, T.-H. Lin, M.-H. Jao, C.-M. Chuang, S.-Y. Chang, Y.-C. Huang, Y.-T. Shao, C.-Y. Chen, C.-J. Su, U.S. Jeng, Y.-F. Chen, W.-F. Su, Nanoparticle-tuned self-organization of a bulk heterojunction hybrid solar cell with enhanced performance, ACS Nano 6 (2) (2012) 1657–1666.
[10] Z. Xiao, Y. Yuan, B. Yang, J. VanDerslice, J. Chen, O. Dyck, G. Duscher, J. Huang, Universal formation of compositionally graded bulk heterojunction for efficiency enhancement in organic photovoltaics, Adv. Mater. 26 (19) (2014) 3068–3075.
[11] C. Gu, Y. Chen, Z. Zhang, S. Xue, S. Sun, C. Zhong, H. Zhang, Y. Lv, F. Li, F. Huang, Y. Ma, Achieving high efficiency of PTB7-based polymer solar cells via integrated optimization of both anode and cathode interlayers, Adv. Energy Mater. 4 (8) (2014) 1301771.
[12] L.K. Jagadamma, M. Al-Senani, A. El-Labban, I. Gereige, G.O. Ngongang Ndjawa, J.C.D. Faria, T. Kim, K. Zhao, F. Cruciani, D.H. Anjum, M.A. McLachlan, P.M. Beaujuge, A. Amassian, Polymer solar cells with efficiency >10% enabled via a facile solution-processed Al-doped ZnO electron transporting layer, Adv. Energy Mater. 5 (12) (2015) 1500204.
[13] S. Woo, W. Hyun Kim, H. Kim, Y. Yi, H.-K. Lyu, Y. Kim, 8.9% single-stack inverted polymer solar cells with electron-rich polymer nanolayer-modified inorganic electron-collecting buffer layers, Adv. Energy Mater. 4 (7) (2014) 1301692.
[14] M. Girtan, M. Rusu, Role of ITO and PEDOT: PSS in stability/degradation of polymer:fullerene bulk heterojunctions solar cells, Sol. Energy Mater. Sol. Cells 94 (3) (2010) 446–450.
[15] E. Voroshazi, B. Verreet, A. Buri, R. Müller, D. Di Nuzzo, P. Heremans, Influence of cathode oxidation via the hole extraction layer in polymer:fullerene solar cells, Org. Electron 12 (5) (2011) 736–744.
[16] H.C. Wong, Z. Li, C.H. Tan, H. Zhong, Z. Huang, H. Bronstein, I. McCulloch, J.T. Cabral, J.R. Durrant, Morphological stability and performance of polymer–fullerene solar cells under thermal stress: the impact of photoinduced PC60BM oligomerization, ACS Nano 8 (2) (2014) 1297–1308.
[17] Z. Sun, K. Xiao, J.K. Keum, X. Yu, K. Hong, J. Browning, I.N. Ivanov, J. Chen, J. Alonzo, D. Li, B.G. Sumpter, E.A. Payzant, C.M. Rouleau, D.B. Geohegan, PS-b-P3HT copolymers as P3HT/PCBM interfacial compatibilizers for high efficiency photovoltaics, Adv. Mater 23 (46) (2011) 5529–5535.
[18] H.-W. Liu, D.-Y. Chang, W.-Y. Chiu, S.-P. Rwei, L. Wang, Fullerene bisadduct as an effective phase-separation inhibitor in preparing poly(3-hexylthiophene)-[6,6]-phenyl-C_{61}-butyric acid methyl ester blends with highly stable morphology, J. Mater. Chem. 22 (31) (2012) 15586–15591.
[19] C.-Y. Chen, C.-S. Tsao, Y.-C. Huang, H.-W. Liu, W.-Y. Chiu, C.-M. Chuang, U.S. Jeng, C.-J. Su, W.-R. Wu, W.-F. Su, L. Wang, Mechanism and control of structural evolution of polymer solar cell from bulk heterojunction to thermally unstable hierarchical structure, Nanoscale 5 (16) (2013) 7629–7638.
[20] C.-P. Chen, C.-Y. Huang, S.-C. Chuang, Highly thermal stable and efficient organic photovoltaic cells with crosslinked networks appending open-cage fullerenes as additives, Adv. Funct. Mater. 25 (2) (2015) 207–213.
[21] B. Meng, Z. Wang, W. Ma, Z. Xie, J. Liu, L. Wang, A cross-linkable donor polymer as the underlying layer to tune the active layer morphology of polymer solar cells, Adv. Funct. Mater. 26 (2) (2015) 226–232.
[22] F. Ouhib, M. Tomassetti, J. Manca, F. Piersimoni, D. Spoltore, S. Bertho, H. Moons, R. Lazzaroni, S. Desbief, C. Jerome, C. Detrembleur, Thermally stable bulk heterojunction solar cells based on cross-linkable acrylate-functionalized polythiophene diblock copolymers, Macromolecules 46 (3) (2013) 785–795.
[23] H.-C. Cha, Y.-C. Huang, F.-H. Hsu, C.-M. Chuang, D.-H. Lu, C.-W. Chou, C.-Y. Chen, C.-S. Tsao, Performance improvement of large-area roll-to-roll slot-die-coated inverted polymer solar cell by tailoring electron transport layer, Sol. Energy Mater. Sol. Cells 130 (2014) 191–198.
[24] S.H.M. Kröger, J. Meyer, T. Riedl, W. Kowalsky, A. Kahn, Role of the deep-lying electronic states of MoO3 in the enhancement of hole-injection in organic thin films, Appl. Phys. Lett. 95 (2009) 123301.
[25] M.T. Greiner, M.G. Helander, W.-M. Tang, Z.-B. Wang, J. Qiu, Z.-H. Lu, Universal energy-level alignment of molecules on metal oxides, Nat. Mater. 11 (1) (2012) 76–81.
[26] Y.-C. Huang, H.-C. Chia, C.-M. Chuang, C.-S. Tsao, C.-Y. Chen, W.-F. Su, Facile hot solvent vapor annealing for high performance polymer solar cell using spray process, Sol. Energy Mater. Sol. Cells 114 (0) (2013) 24–30.
[27] Y.-C. Huang, C.-S. Tsao, H.-C. Cha, C.-M. Chuang, C.-J. Su, U.S. Jeng, C.-Y. Chen, Correlation between hierarchical structure and processing control of large-area spray-coated polymer solar cells toward high performance, Sci. Rep. 6 (2016) 20062.
[28] S. Chambon, L. Derue, M. Lahaye, B. Pavageau, L. Hirsch, G. Wantz, MoO3 thickness, thermal annealing and solvent annealing effects on inverted and direct polymer photovoltaic solar cells, Materials 5 (12) (2012) 2521–2536.
[29] W. Greenbank, L. Hirsch, G. Wantz, S. Chambon, Interfacial thermal degradation in inverted organic solar cells, Appl. Phys. Lett. 107 (26) (2015) 263301.
[30] E. Vitoratos, S. Sakkopoulos, N. Paliatsas, K. Emmanouil, S.A. Choulis, Conductivity degradation study of PEDOT: PSS films under heat treatment in helium and atmospheric air, Open J. Org. Polym. Mater. 2 (01) (2012) 7–11.
[31] M.O. Reese, S.A. Gevorgyan, M. Jørgensen, E. Bundgaard, S.R. Kurtz, D.S. Ginley, D.C. Olson, M.T. Lloyd, P. Morvillo, E.A. Katz, A. Elschner, O. Haillant, T.R. Currier, V. Shrotriya, M. Hermenau, M. Riede, K.R. Kirov, G. Trimmel, T. Rath, O. Inganäs, F. Zhang, M. Andersson, K. Tvingstedt, M. Lira-Cantu, D. Laird, C. McGuiness, S. Gowrisanker, M. Pannone, M. Xiao, J. Hauch, R. Steim, D.M. DeLongchamp, R. Rösch, H. Hoppe, N. Espinosa, A. Urbina, G. Yaman-Uzunoglu, J.-B. Bonekamp, A.J.J.M. van Breemen, C. Girotto, E. Voroshazi, F.C. Krebs, Consensus stability testing protocols for organic photovoltaic materials and devices, Sol. Energy Mater. Sol. Cells 95 (5) (2011) 1253–1267.